Effects of Moist Convection on Mesoscale Predictability

F. ZHANG

Department of Atmospheric Sciences, Texas A&M University, College Station, Texas

CHRIS SNYDER AND RICHARD ROTUNNO

National Center for Atmospheric Research, Boulder, Colorado*

(Manuscript received 6 May 2002, in final form 11 December 2002)

ABSTRACT

In a previous study by the authors, it was shown that the problematic numerical prediction of the 24–25 January 2000 snowstorm along the east coast of the United States was in some measure due to rapid error growth at scales below 500 km. In particular they found that moist processes were responsible for this strong initial-condition sensitivity of the 1–2-day prediction of mesoscale forecast aspects. In the present study they take a more systematic look at the processes by which small initial differences (''errors'') grow in those numerical forecasts. For initial errors restricted to scales below 100 km, results show that errors first grow as small-scale differences associated with moist convection, then spread upscale as their growth begins to slow. In the context of mesoscale numerical predictions with 30-km resolution, the initial growth is associated with nonlinearities in the convective parameterization (or in the explicit microphysical parameterizations, if no convective parameterization is used) and proceeds at a rate that increases as the initial error amplitude decreases. In higher-resolution (3.3 km) simulations, errors first grow as differences in the timing and position of individual convective cells. Amplification at that stage occurs on a timescale on the order of 1 h, comparable to that of moist convection. The errors in the convective-scale motions subsequently influence the development of meso- and larger-scale forecast aspects such as the position of the surface low and the distribution of precipitation, thus providing evidence that growth of initial errors from convective scales places an intrinsic limit on the predictability of larger scales.

1. Introduction

It is widely appreciated that the difficulty of numerical weather prediction (NWP) arises in part because the evolution of the atmosphere depends sensitively on initial conditions; that is, small differences in the initial state produce solutions that diverge over time. One can, in principle, always extend the lead time of skillful forecasts by simply improving the estimate of the initial state (say by improving the observing network). Lorenz (1969), however, argued that forecast errors would grow more rapidly as the initial estimate was improved and successively smaller scales were resolved. He conjectured that this increasingly rapid error growth would impose an inherent, finite limit to the predictability of the atmosphere, as successive refinements of the initial estimate would yield smaller and smaller increments to the length of a skillful forecast. While the notion that there is a limit to atmospheric predictability is now widely accepted, relatively little is known about the mechanisms by which small-scale errors grow and influence larger scales. In this paper, we investigate through integrations of a high-resolution regional NWP model the hypotheses that moist convection is a primary mechanism for forecast-error growth at sufficiently small scales, and that convective-scale errors contaminate the mesoscale within lead times of interest to NWP, thus effectively limiting the predictability of the mesoscale.

Existing demonstrations of the limit of predictability are all based on statistical closure models of homogeneous isotropic turbulence (Lorenz 1969; Leith 1971; Leith and Kraichnan 1972; Metais and Lesieur 1986). These closure models indicate, in agreement with simple dimensional arguments (Lorenz 1969; Lilly 1972), that the energy-cascading inertial range of either two- or three-dimensional turbulence has an intrinsic, finite limit of predictability, while the two-dimensional enstrophy-cascading inertial range does not. Direct numerical simulations provide some support for predictability results from closure models in the two-dimensional entrophy-

* The National Center for Atmospheric Research is sponsored by the National Science Foundation.

Corresponding author address: Dr. Fuqing Zhang, Department of Atmospheric Sciences, Texas A&M University, 3150 TAMU, College Station, TX 77843-3150.
E-mail: fzhang@tamu.edu

cascading range (Lilly 1972; Boffetta et al. 1996). The relevance of any of these calculations to the atmospheric mesoscale, however, is uncertain, as those scales are characterized not by homogeneous turbulence but by highly intermittent phenomena such as fronts and organized moist convection.

Work focusing directly on mesoscale predictability began with Anthes et al. (1985). They noted little divergence of simulations from different initial conditions in a limited-area mesoscale model; in fact, the growth of forecast differences was slower even than that found in global models at the time. Such slow growth of forecast differences was subsequently determined to be caused by the combined effects of fixed lateral boundary conditions, relatively strong numerical dissipation, and adjustment of the imposed initial differences through radiation of inertia–gravity waves (Errico and Baumhefner 1987; Vukicevic and Errico 1990). Ehrendorfer and Errico (1995) calculated forecast-difference evolution without the effects of moisture and found that the fastest growing perturbations (i.e., the leading singular vectors) in a mesoscale model were similar to those in lower-resolution global models. None of these studies suggested distinct mechanisms for error growth at meso- or smaller scales.

More recently, however, forecast difference growth associated with moist processes and small scales has been found by Ehrendorfer et al. (1999) and Zhang et al. (2002, hereafter ZSR). [See also Toth and Kalnay (1997), who note similar behavior in a global model.] ZSR studied the ''surprise'' snowstorm of 24–25 January 2000, which brought abundant and underforecasted snowfall to the east coast of the United States between North Carolina and Washington, D.C. In limited-area simulations initialized with analyses from various operational centers, they found that differences between simulations grew rapidly at scales below 500 km, and that the difference growth was much slower if the effects of latent heat release were turned off in both simulations. These results of ZSR suggest that, with 30-km resolution, mesoscale models begin to exhibit error growth with characteristics similar to those identified by Lorenz (1969) as intrinsically limiting predictability: forecast differences in ZSR grew much more rapidly, and at smaller scales, than would be found in models with coarser resolution, and growth rates increased as the amplitude of the initial difference decreased.

The growth of forecast differences in the case of ZSR is examined in more detail here. Key issues to be addressed in the present study are 1) the mechanisms underlying rapid growth of small-scale differences in the ZSR simulations, particularly the role of moist convection and its parameterization; and 2) whether difference growth rates continue to increase as resolution is increased, as would be expected for a system with limited predictability. As will be seen, the answers to these questions indicate that present high-resolution simulations and forecasts of precipitation on the mesoscale are influenced significantly by rapid error growth at the smallest resolved scales, and thus these forecast systems are approaching their inherent limits of predictability.

As in ZSR, our numerical experiments consist of integrating the mesoscale model from pairs of slightly different initial conditions and examining the evolution of the difference between the two simulations. In order to focus on the difference growth from the smallest scales, the initial difference here is chosen to be a monochromatic perturbation near the smallest resolved scale of the model. We also extend the results of ZSR by performing experiments with an inner grid of 3.3-km resolution on which moist convection is explicitly (though marginally) resolved, rather than represented by a parameterization.

The numerical experiments and the mesoscale model are described in greater detail in the next section. We then present results at 30-km resolution in section 3, and at 3.3-km resolution in section 4. A summary of results and further discussion appear in section 5.

2. Experimental design

The same surprise snowstorm of 24–25 January 2000 as studied in ZSR is further investigated in this study. The medium-range forecasts and predictability of this event are examined in Langland et al. (2002). A brief synoptic description of the storm can be found in ZSR (their Fig. 2).

The two-way nested National Center for Atmospheric Research–The Pennsylvania State University (NCAR–PSU) nonhydrostatic fifth-generation mesoscale model (MM5) version 2 was used for this study (Dudhia 1993). The model configurations are exactly the same as used in ZSR. The highest-resolution simulations employed three model domains with 30, 10, and 3.3 km grid resolutions. The 30-km coarse domain employs 190×120 grid points with 27 vertical layers, covering the entire continental United States, while the number of grid points for both the 10- and 3.3-km nested domains is 241×181 (Fig. 1). The Mellor–Yamada planetary boundary layer scheme (Mellor and Yamada 1982) and Reisner microphysics scheme with graupel (Reisner et al. 1998) are used for all three domains. Domains 1 and 2 use the Grell cumulus parameterization scheme (Grell 1993) while domain 3 is fully explicit. Several low-resolution experiments, which used only the 30-km coarse domain, were also performed.

The unperturbed control simulations were initialized at 0000 UTC 24 January 2000 with the operational Eta model 104-grid ($\sim$85-km horizontal resolution) data reanalyzed with conventional observations. We will denote the high-resolution control by Cntl-3.3km and the low-resolution by Cntl-30km. Both these control simulations and the perturbed simulations described below use the operational Eta model 104-grid forecasts, updated every 6 h, as lateral boundary conditions.

Simulations from perturbed initial conditions were

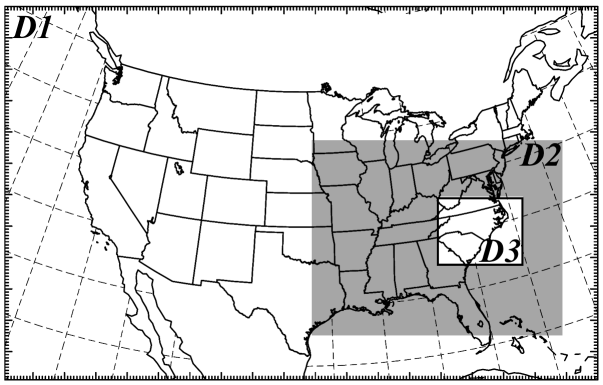

FIG. 1. The relative locations of MM5 model domains. The grid resolutions of domain 1 (D1), domain 2 (D2), and domain 3 (D3) are 30, 10, and 3.3 km, respectively; D3 is moveable with the snapshot location valid at 0000 UTC 25 Jan 2000.

also performed (Pert-3.3km and Pert-30km, respectively, for high and low resolution). Since our interest lies in the growth of forecast differences from small scales, the initial perturbations have the form of a height-independent, monochromatic disturbance in temperature given by

$$T' = T_0 \sin[(i + j)\pi/2], \quad (1)$$

where i and j are indices in the x and y directions, respectively, on the coarse 30-km grid. (Thus, the total wavelength is $2\sqrt{2}$ times the horizontal grid spacing, or roughly 85 km.) In the high-resolution simulations, the perturbation (1) is first added to the control initial conditions on the coarse grid and the finer grids are initialized by interpolation from the coarse grid. The disturbance amplitude T_0 is set to 0.1 K in Pert-30km and 0.5 K in Pert-3.3km; additional experiments with other values for T_0 (ranging from 1.0 to 0.001 K) have also been performed and will be discussed below.

3. Error growth in the low-resolution experiments

We begin by examining the evolution of forecast differences at low resolution (i.e., the difference between Cntl-30km and Pert-30km). After 6 h of simulation (Fig. 2a), the initial, monochromatic disturbance given by (1) has decayed everywhere except for a small region near the coasts of Louisiana and Alabama, where there has been an increase locally in the difference. Figure 2b shows that the difference remains localized at the 12-h forecast time, although it has spread over a larger area and the spatial scale of its variations has increased. The maximum amplitude of the difference has also doubled. By 24 h (Fig. 2c), the difference field has spread over a substantial portion of the domain, its spatial scale has continued to increase, and the maximum temperature difference at 300 hPa has grown to a magnitude of ~2.5 K, nearly 25 times stronger than the initial perturbation.

The simulation differences in other variables and at other levels below 250 hPa behave similarly. In order

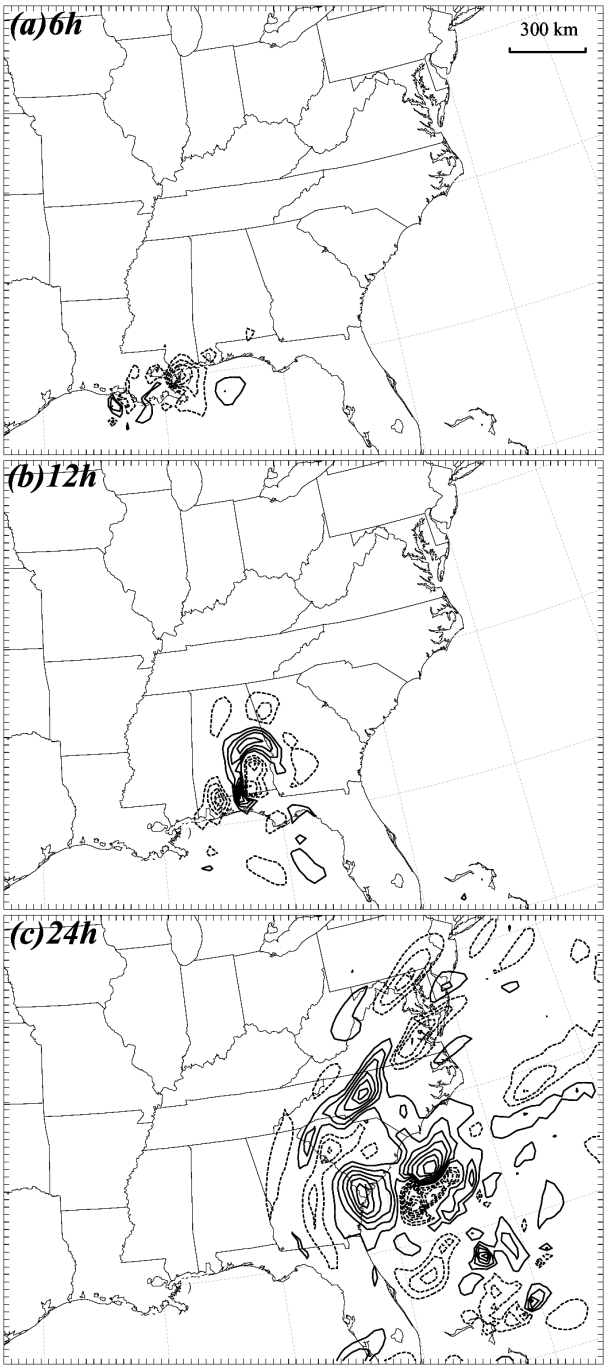

FIG. 2. The 300-hPa temperature difference between Cntl-30km and Pert-30km at (a) 6-, (b) 12-, and (c) 24-h forecast time. Contour intervals are (a) 0.1 K and (b) and (c) 0.2 K; dashed contours indicate negative values.

to quantify this, we employ an integrated norm for the differences, namely, the difference total energy (DTE) per unit mass defined by

$$\text{DTE} = 1/2 \sum (U'^2_{ijk} + V'^2_{ijk} + \kappa T'^2_{ijk}), \quad (2)$$

U', V', and T' are the difference wind components and

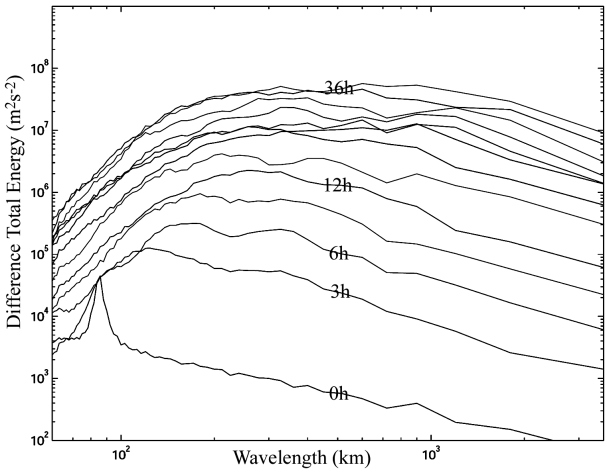

FIG. 3. Power spectra of the DTE (in $m^2\ s^{-2}$) between Cntl-30km and Pert-30km plotted every 3 h.

difference temperature between two simulations, $\kappa = C_p/R$, and i, j, and κ run over x, y, and σ grid points.

A power-spectrum analysis of DTE is shown in Fig. 3. As suggested by Fig. 2a, the growth of the difference field is most rapid over the first 3 h (with DTE increasing by a factor of more than 10) and then slows steadily over the rest of the forecast interval to 36 h. Over this same initial period, the differences also spread to larger scales from the 85-km wavelength imposed by (1); such spectral behavior is at least partly a signature of increasing spatial localization of the differences as they grow locally over Louisiana and decay elsewhere. (A localized patch of noise appears as a delta function to sufficiently long waves, and thus its Fourier transform will have a peak at the scale of the noise and roughly constant amplitude for wavelengths larger than a few patch sizes.) Beyond the first 3 h, the spectra show that differences grow at all scales. Over the same interval, the peak of the spectrum gradually migrates with time to larger scales (600~900 km after 36 h) as both the scale of variation of the differences and their areal extent increase (Fig. 2c).

At no point in the simulations does the spectral peak advance beyond 1000 km. In the experiments reported in ZSR, differences at scales greater than 1000 km typically decayed, owing to the fact that both control and perturbed runs used the same lateral boundary conditions; this effect is well known from previous studies (Vukicevic and Errico 1990 and references therein). We believe that the use of identical boundary conditions also inhibits the difference growth beyond 1000 km in the latter stages of the present simulations, as is evident in Fig. 3.

As noted in ZSR and also evident in Fig. 3, the difference growth rate, especially at smaller scales, is larger at smaller difference amplitude. To see this more clearly, we have performed several experiments configured exactly the same as Pert-30km except using $T_0 = 1.0$, 0.5, 0.01, and 0.001 K in (1). Figure 4 shows the evolution of the error growth in these experiments. Clearly, the smaller the initial difference is, the faster it grows; this

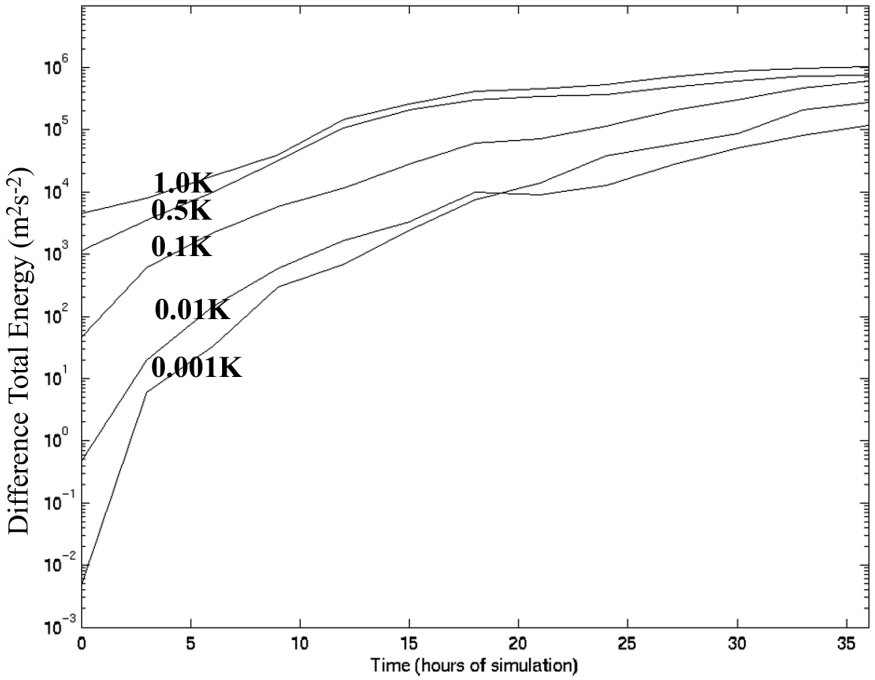

FIG. 4. Evolution of DTE (in $m^2\ s^{-2}$) in experiments with idealized perturbations of different magnitudes in the initial temperature field. Curves are labeled with the values of T_0 used in (1).

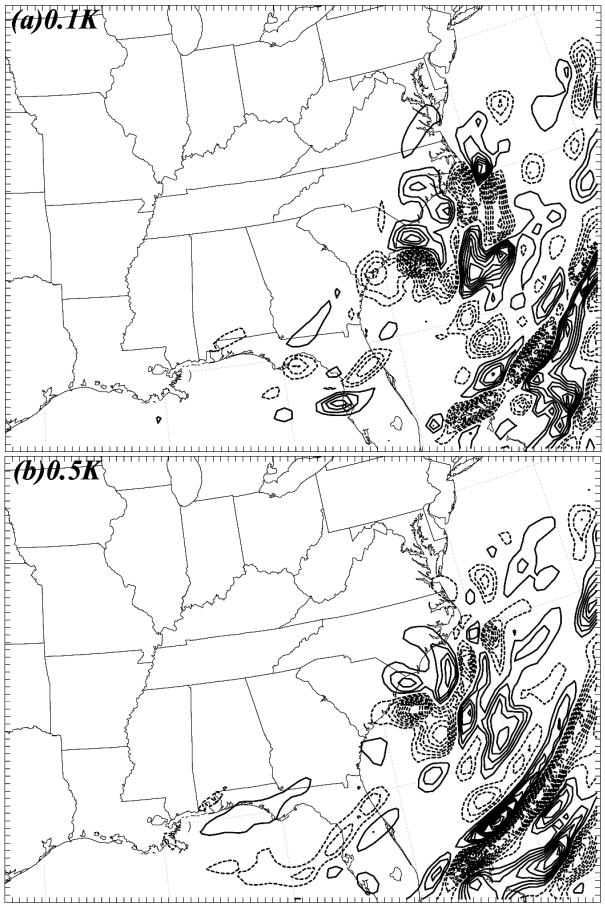

FIG. 5. (a) The 36-h accumulated precipitation difference between Cntl-30km and Pert-30km. (b) As in (a) but the initial perturbation amplitude changed from 0.1 to 0.5 K. Contour intervals are (a) 2 mm and (b) 5 mm, and dashed contours indicate negative values.

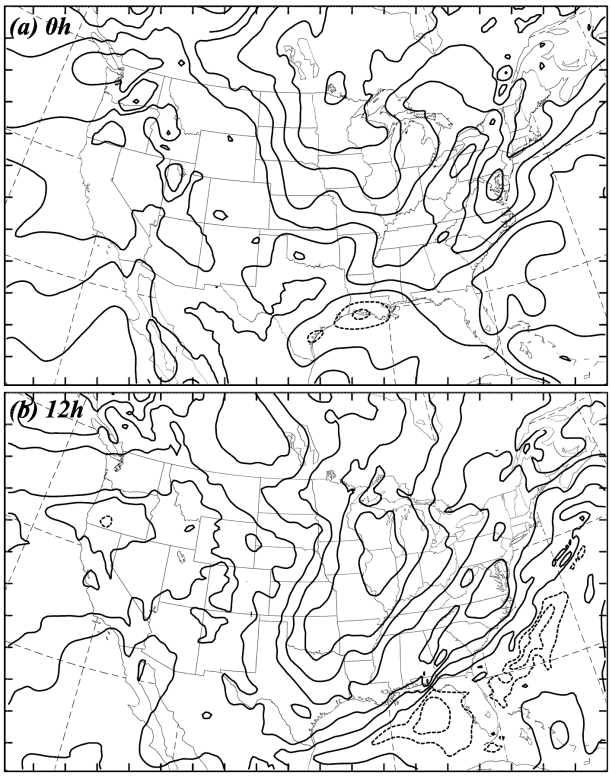

FIG. 6. The lifted index (contour interval 2 K, negative values dashed) estimated from the Cntl-30km simulation valid at (a) 0000 and (b) 1200 UTC 24 Jan 2000.

behavior indicates that the mechanisms for error growth are nonlinear. This dependence of error growth rate on the amplitude is consistent with the physical arguments made by Lorenz (1969) for systems in which small-amplitude error in small scales ultimately limits the predictability of larger scales.

The forecast sensitivity to very small errors in the initial condition is manifested not only in the temperature and wind, but also in the short-range mesoscale precipitation forecast. Figure 5a shows that the maximum 36-h accumulated precipitation difference between Cntl-30km and Pert-30km can be as large as 40 mm and extends over much of the Atlantic coast. Even larger precipitation difference results when increasing the initial error amplitudes in Pert-30km from 0.1 to 0.5 K (Fig. 5b). These 36-h precipitation forecast differences (e.g., over the Carolinas) are significant compared to the observed accumulated precipitation over the same period (Fig. 1 in ZSR).

Sensitivity experiments in ZSR showed that moist processes were essential contributors to the rapid divergence of forecasts. To gain some insight into the processes at work, we show in Fig. 6 the lifted index (see p. 447 of Bluestein 1993 for definition) from the Cntl-30km simulation valid at 0000 and 1200 UTC 24 January 2000 (i.e., at 0 and 12 h into the simulation). Initially, there is a relatively small region of negative lifted index (indicating convective instability) near the coast of Louisiana (Fig. 6a). The convectively unstable region corresponds closely to the region of difference growth evident in Fig. 2a; in fact, after 3 h (not shown), the differences are almost completely confined to the conditionally unstable region. This correspondence suggests that moist convection, or at least its parameterized version in the model, is the key to the initial localized error growth. At later times, some correspondence remains, but it is much less pronounced (cf. Figs. 2b,c and 6b).

To further investigate the role of moist convection in producing rapid error growth, a set of ''fake dry'' experiments has been performed in which the latent heat of condensation is set to zero; that is, the fake dry experiments are identical to the standard experiments Cntl-30km and Pert-30km except that the diabatic contribution from moist processes is ignored (in both simulations). Figure 7 shows that the growth of DTE in the fake dry simulation is greatly reduced compared with that of the standard, moist simulations; this is further evidence for the direct dependence of difference growth

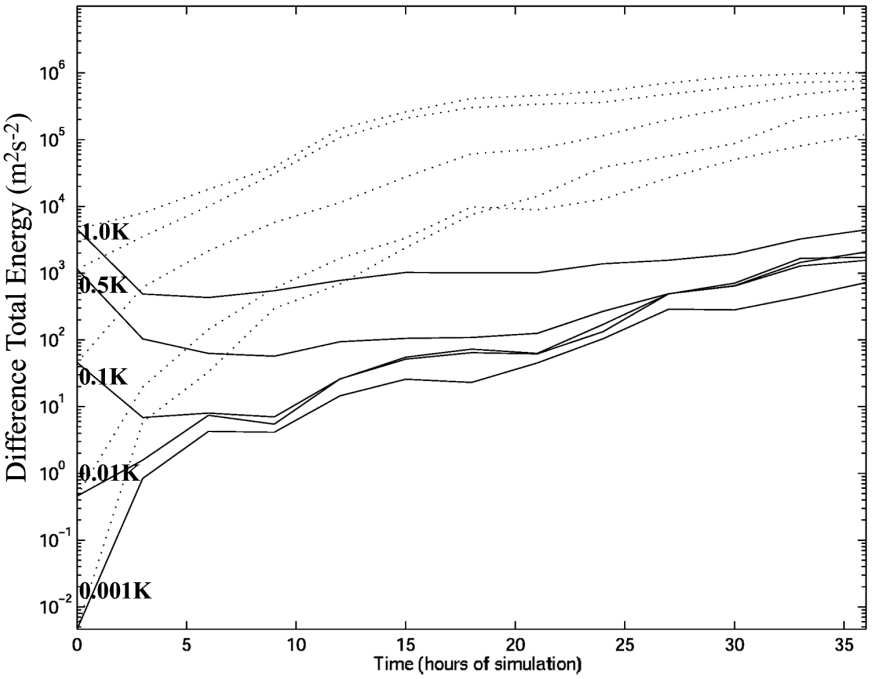

FIG. 7. As in Fig. 4 but for the fake dry experiments (solid curves). The dotted curves indicate the corresponding error evolution in the moist experiments.

on convective instability. Note, however, that even in the fake dry experiments, the differences still behave differently at different amplitudes and can grow starting from sufficiently small initial amplitude (e.g., $T_0 = 0.001$ shown in Fig. 7).

Forecast differences in both the fake dry (not shown) and standard, moist simulations (Fig. 2) are dominated by variations near the grid scale, especially at early times. This observation suggests that the physical parameterizations may play a role in the difference growth. In addition, the thresholds and ''on–off'' switches present in most parameterizations are a known source of nonlinearity for small initial differences (Errico and Raeder 1999 and references therein), consistent with the strong dependence of the difference growth on amplitude (Figs. 4 and 7).

The nonlinearity of the parameterizations, and their potential influence on difference growth arises from the fact that, at many times and locations, the model forecast fields lie close to a critical value where small perturbations to the solution can cause the parameterization to cross a threshold and thereby discontinuously change the response associated with that perturbation. With this picture in mind, we have examined the difference evolution within the first 2 h of a simulation with a very small amplitude initial perturbation (specifically, a simulation as in Pert-30km but with $T_0 = 0.001$ K). Figure 8 shows that the maximum temperature difference in this case increases by a factor of 40 over the first 10 min. This initial growth is associated with slight differences in the initial temperature turning on the cumulus parameterization at one (or a few) grid points in one simulation but not in the other, which can then induce a temperature difference of ~0.01–0.1 K at those grid points over several model time steps, regardless of the size of the initial difference.

An additional question is whether the rapid growth of small differences is a pathological property of the Grell convective scheme used in the simulations. There is strong evidence that this is not the case. First, qualitatively similar (but significantly slower) growth of small differences occurs in the fake dry experiments (Fig. 7), apparently through the thresholds in other physical parameterizations (e.g., for the boundary layer). In addition, we have performed a set of experiments without convective parameterization in either the control or perturbed simulations; that is, moist processes are represented in these experiments only by explicit grid-scale microphysics. As shown by the circled points in Fig. 8, the growth of the maximum temperature perturbation is somewhat slower with only explicit microphysics, but this difference disappears over the first hour of the simulations. Finally, we also performed experiments substituting the scheme of Kain and Fritsch (1990) for the Grell (1993) convective scheme; the error-growth characteristics (not shown) are quantitatively similar to the simulation using the Grell scheme.

4. Error growth in higher-resolution simulations

The previous section demonstrates that initial differences near the grid scale in the 30-km simulations grow

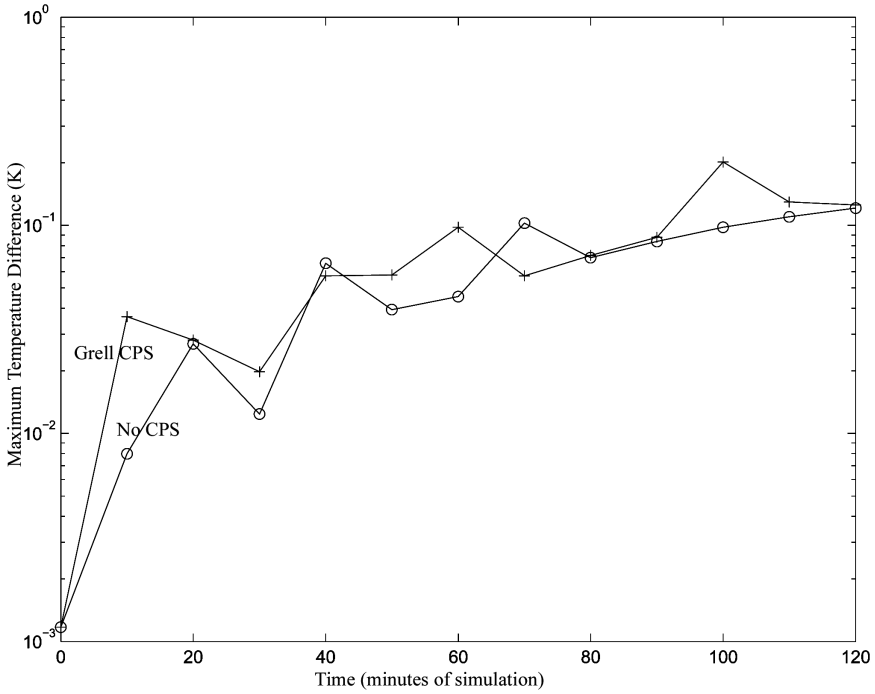

FIG. 8. Maximum temperature difference from Cntl-30km as a function of time for two perturbed simulations, one using the Grell convective parameterization scheme (CPS) as in Pert-30km (+) and the other using no convective parameterization (circles). In both simulations, the initial perturbation is given by (1) with $T_0 = 0.001$ K.

rapidly, spread upscale over the first day of simulation, have a spectral peak at wavelengths of several hundred kilometers, and evolve with significant nonlinearity even for small initial amplitudes. It is natural to ask whether these results, which were obtained with parameterized moist convection, are representative of the real atmosphere or of higher-resolution simulations that resolve moist convection.

To address this question, triply nested simulations (Cntl-3.3km, Pert-3.3km) were performed as described in section 2 using a 3.3-km resolution on the inner grid. The perturbed simulation (Pert-3.3km) was initialized, as in the 30-km experiments, with an idealized, monochromatic temperature perturbation given by (1), but with $T_0 = 0.5$ K.

The 300-hPa temperature difference between experiments Cntl-3.3km and Pert-3.3km is shown in Fig. 9 for forecast times of 6, 12, and 30 h. Fields in Fig. 9 (and subsequent figures) are averaged to the 30-km grid for plotting; Figs. 9a–b may thus be compared directly with the 30-km results of Figs. 2a–b, which show the same times. The difference evolution at high resolution has certain qualitative similarities to the lower-resolution results. In particular, the difference field becomes localized over the first 6 h in much the same location (cf. Figs. 2a and 9a), again through a combination of rapid growth where there is convective instability and decay elsewhere. Then, over the next 6 h, the differences spread over a larger area, as did the differences in the 30-km simulations (Figs. 2b and 9b).

Despite these similarities, the 3.3- and 30-km results also differ in important respects. First, the differences grow more rapidly at higher resolution, both increasing their maximum amplitude more quickly and spreading over larger areas. The differences also have larger scale in the 3.3-km simulations, particularly at early times: by 6 h, the temperature difference at high resolution has the form of a dipole roughly 600 km in width, while the differences vary on scales of less than 200 km at low resolution.

Figure 10 shows the power spectrum of DTE at various times in the 3.3-km simulations. Comparing against the results for the 30-km simulations (Fig. 3), it is again clear that the differences at high resolution grow more rapidly and spread to larger scales more quickly. (Note the spectral peak at 600 km at 6 h, consistent with the difference structure shown in Fig. 9.) In addition, the spectra at 1 and 2 h (dotted lines in Fig. 10) indicate that the rapid growth begins on the scale of the initial perturbation, but that differences quickly begin growing at the mesoscale, as evidenced by the distinct spectral peak at 600-km wavelength after 2 h.

The maximum 36-h accumulated precipitation difference between Pert-3.3km and Cntl-3.3km covers a large region of the Atlantic coast and has local maximum of 100 mm (Fig. 11), or more than twice that found

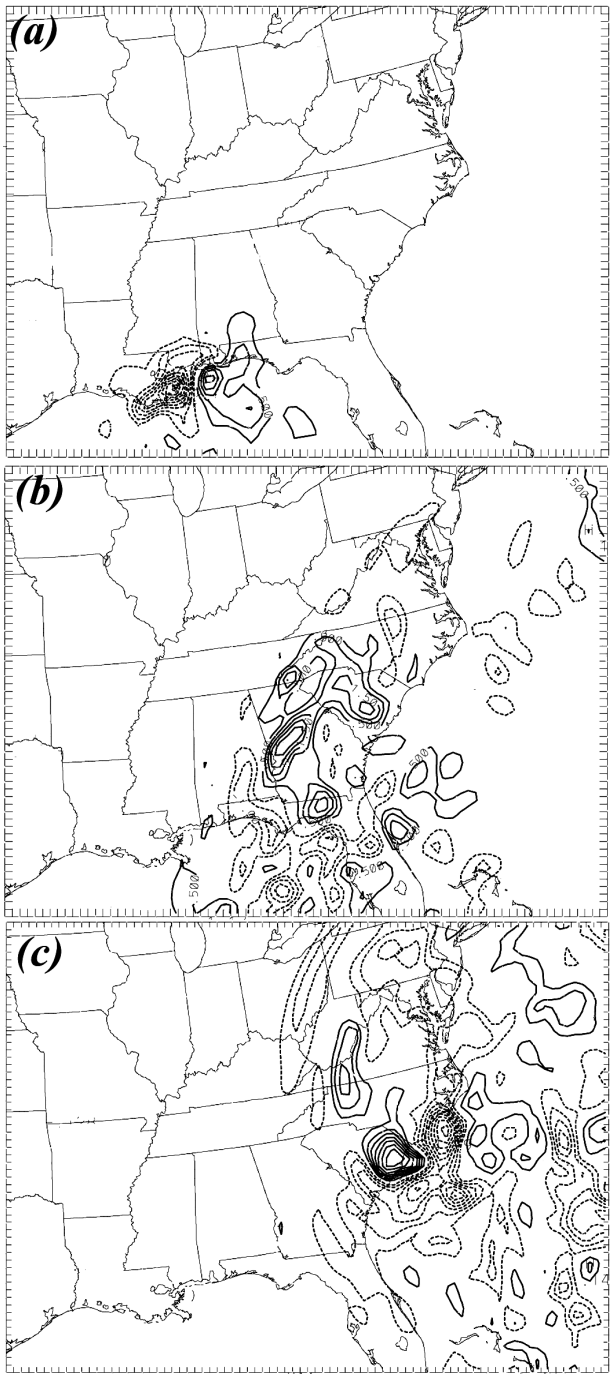

FIG. 9. The 300-hPa temperature difference (contour interval 0.5 K) between Cntl-3.3km and Pert-3.3km after (a) 6, (b) 12, and (c) 30 h of simulation. Fields are shown on the 30-km grid.

in the 30-km simulations (Fig. 5b) even after averaging to the 30-km grid. The precipitation forecast is, again, significantly different with small initial perturbations.

To shed some light on the mechanisms by which model forecasts diverge, we show in Fig. 12 the mean sea level pressure and reflectivity at the 6-, 12-, and 30-h forecast times from Cntl-3.3km (Figs. 12a–c) and Pert-3.3km (Figs. 12d–f). Recall that after 6 h of simulation, the maximum 300-mb temperature difference is ~4.5 K (Fig. 9a). Comparison of Fig. 12a with Fig. 12d shows that the difference between the mean sea level pressure and reflectivity, however, is relatively small at this time. Examination of the simulations at 1 and 2 h (not shown) indicates that the perturbations in Pert-3.3km are sufficiently strong that the localized moist convection over the Gulf coast is triggered earlier. Thus, the convection and the associated outflow boundary at 6 h are stronger and advance approximately 50 km farther to the east as compared with their counterparts in Cntl-3.3km (Figs. 12a,d). While the difference in the upper-level fields is spreading over a broader area (Fig. 9b), the difference in the sea level pressure fields and the precipitation bands (indicated by the model-derived reflectivity) be-

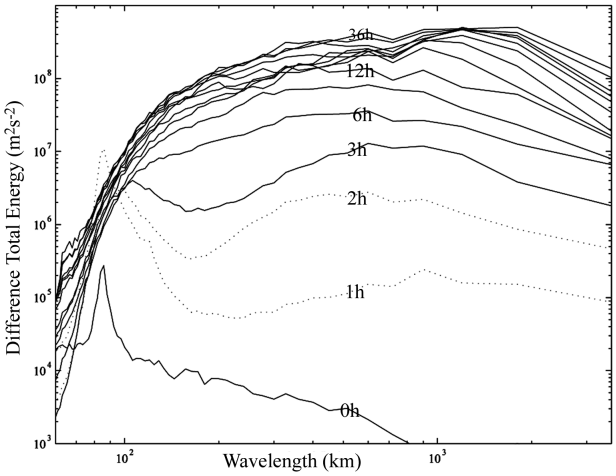

FIG. 10. As in Fig. 3, except for differences between Cntl-3.3km and Pert-3.3km on the 30-km grid, and showing spectra after 1 and 2 h of simulation (dotted lines).

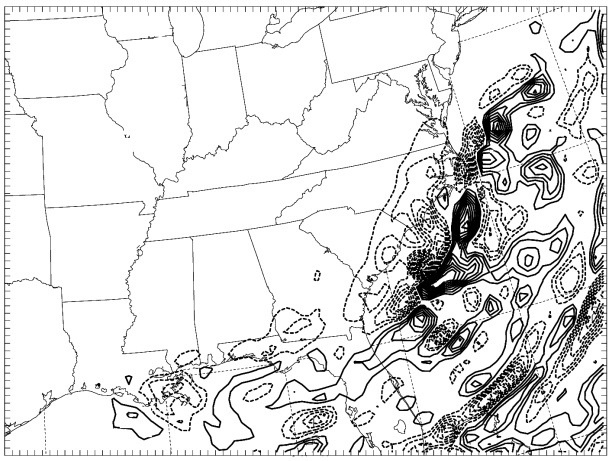

FIG. 11. The 36-h accumulated precipitation difference (contour interval 0.5 cm) between Cntl-3.3km and Pert-3.3km on the 30-km grid. The contour interval is 0.5 cm and negative values are dashed.

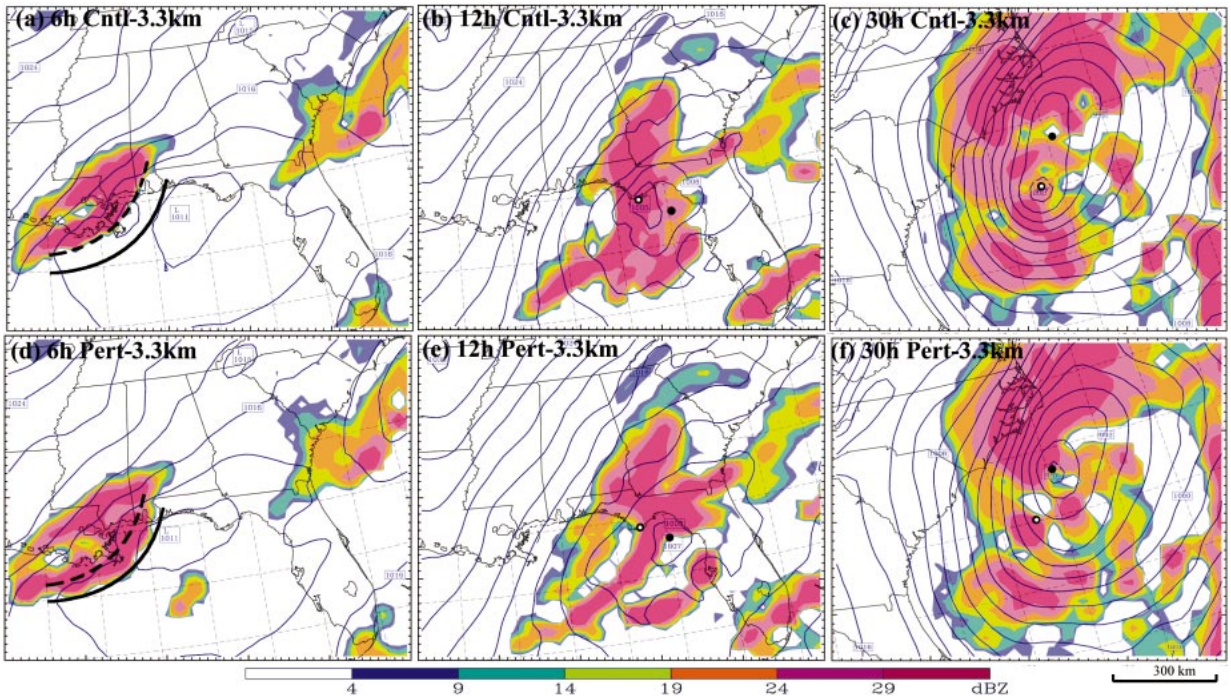

FIG. 12. Comparison of mean sea level pressure (contour interval 4 hPa) and simulated reflectivity (dBZ, colored) on the 30-km grid for Cntl-3.3km and Pert-3.3km. Simulations are shown at (a), (d) 6 h, (b), (e) 12 h, and (c), (f) 30 h. Thick curves in (a) and (b) denote the relative locations of the convective outflow boundary in Cntl-3.3km (dashed) and Pert-3.3km (solid). The dots in (b), (c), (e), and (f) denote the locations of the primarily surface cyclone centers in Cntl-3.3km (open dots) and Pert-3.3km (solid dots).

comes apparent at 12 h (Figs. 12b,e), as the developing surface low is displaced by ~75 km with ~2.0 hPa difference in strength. Subsequent evolution of those differences results in a ~150 km displacement of the cyclone center in the 30-h simulation (Figs. 12c,f); the significant difference in the reflectivity patterns along the Atlantic coast is consistent with the large 36-h accumulated precipitation difference shown in Fig. 11.

Figure 12 suggests that, by 30 h of simulation, the forecast differences have made a transition from convective-scale, unbalanced motions to larger-scale, balanced motions. This is evident, for example, in the differences in the subsynoptic-scale structure of the surface cyclone at 30 h (Figs. 12c,f). The development of differences in the potential vorticity (PV) at 300 hPa provides further evidence of this transition (Fig. 13). At 6 and 12 h (Figs. 13a,b), the PV differences are poorly organized and show little relation to the PV of the control simulation, beyond the localization of the differences above the conditionally unstable region southeast of the upper trough, which is associated with the tongue of high PV extending through the central United States. By 30 h (Fig. 13c), however, the PV differences are clearly organized in long bands stretching along the contours of PV from the control simulation, and these bands occur preferentially where the gradients of control simulation PV are largest.

Potential vorticity differences in the form of bands aligned with the control simulation PV are also characteristic of forecast errors that have grown over $O(1)$ day in a quasigeostrophic model (Snyder et al. 2003). This correspondence with quasigeostrophic results again indicates that the forecast differences at 30 h have not only spread upscale from their origin at convective scales, but also begun to appear to as differences in the balanced, synoptic-scale flow. Thus, the growth at larger scales evident in the difference fields themselves (Figs. 9 and 13) and in the DTE spectra (Fig. 10) is not just the spreading of a localized difference field over a larger area with time, but marks the transition from unbalanced dynamics at convective scales to balanced flow at larger scales.

Finally, we return to the implications of above results for the limits of predictability. The solid line in Fig. 14 shows the evolution of DTE for Pert-3.3km over the first 6 h of simulation. One can estimate a rough timescale from this curve: it increases by about a factor of 40 between the first and third hours of the simulations, which indicates that the differences double in well under an hour (recall that DTE depends on the square of the differences). Thus, even if the forecast model were perfect and the errors in the initial condition confined to convective scales, reducing the initial errors by half would extend the forecast at a given level of skill less than an hour. Again, the increase of error growth rates at small scales implies a decreasing return on any im-

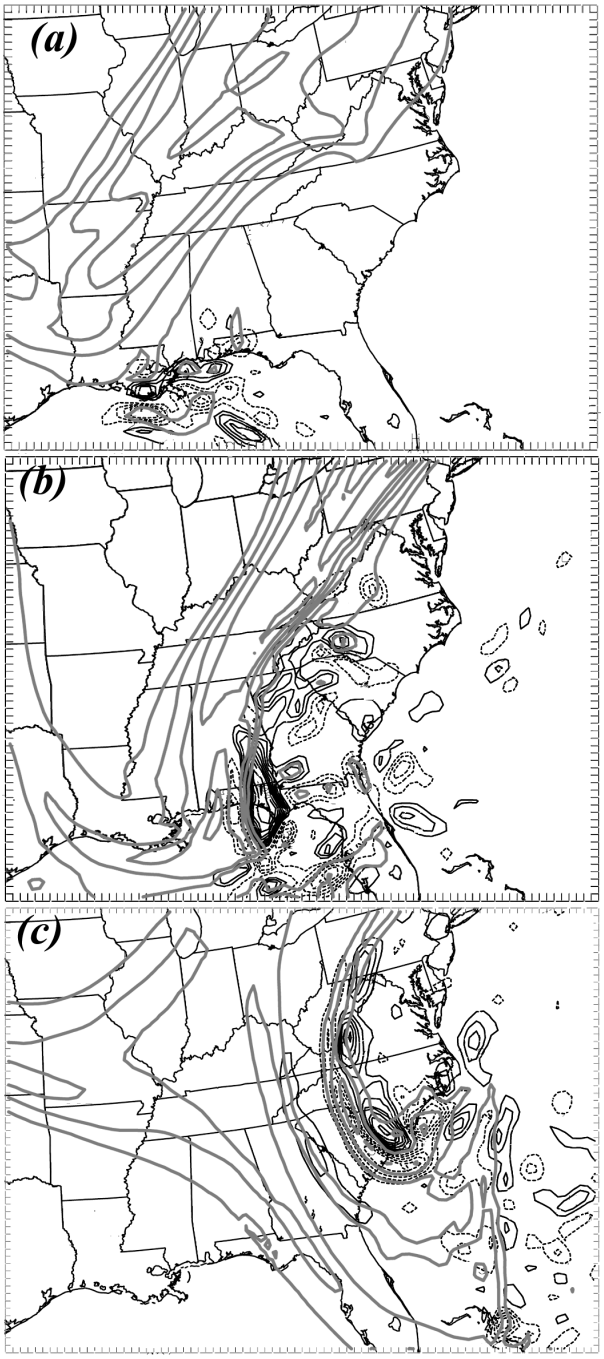

FIG. 13. The 300-hPa PV difference between Cntl-3.3 km and Pert-3.3km (thin lines) at (a)–(c) 6, 12, and 30 h, together with the 300-hPa PV from Cntl-3.3km (thick gray curves). Contour intervals are 0.5 PV units for the difference field (negative values dashed) and 1.5 PV units for the full field; both are shown on the 30-km grid.

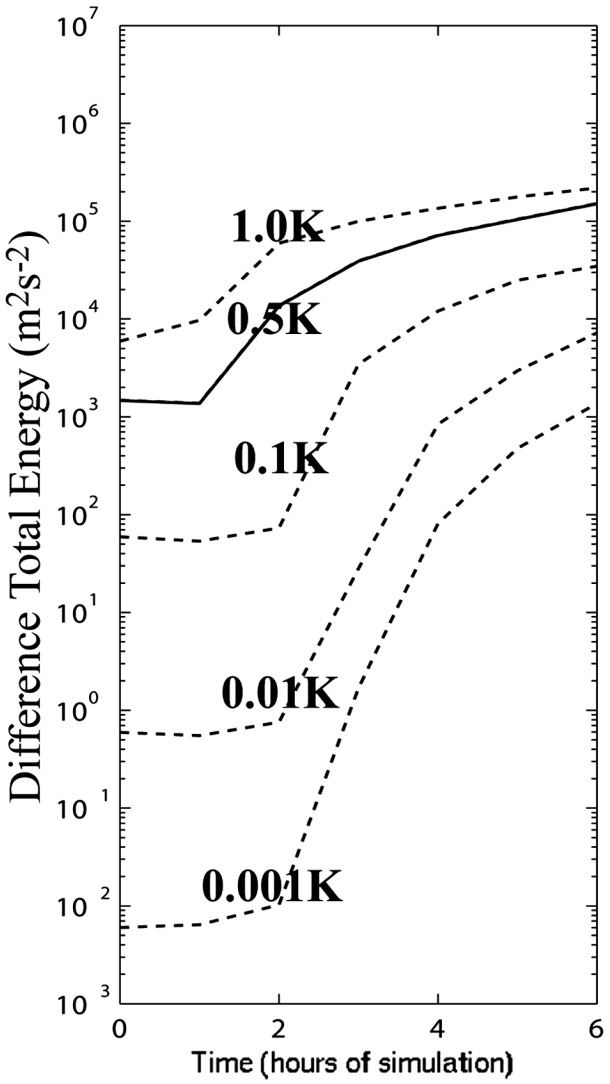

FIG. 14. Evolution of DTE (in $m^2\ s^{-2}$) estimated for differences on the 30-km grid between Cntl-3.3km and high-resolution perturbed simulations with $T_0 = 0.001$, 0.01, 0.1, 0.5, 1.0 K in (1). The solid curve indicates DTE for $T_0 = 0.5$ K (i.e., for Pert-3.3km).

provements to the initial conditions and thus fundamentally limits the predictability of the system.

To illustrate this point more thoroughly, we have performed a sequence of additional perturbed simulations initialized as in Pert-3.3km but with perturbation amplitudes $T_0 = 1$, 0.1, 0.01, 0.001 K in (1). The growth of DTE over the first 6 h for each of these simulations is shown by dotted lines in Fig. 14. Note that, for the smaller values of T_0, the growth of DTE does not begin until the second hour of the simulation. This behavior arises from the finite-amplitude nature of moist convection—sufficiently large initial perturbations can initiate convection and begin growing immediately, while the growth of smaller perturbations must await the onset of convection in the control simulation, which occurs after about an hour. More important, however, is the fact that decreasing the initial perturbation amplitude by a factor of 10 delays the time at which a given amplitude is achieved by less than three hours, consistent with our estimate that the differences should double in less than

an hour. (Consider, for example, the time at which DTE becomes larger than 10^3 m^2 s^{-2} in Fig. 14.) In addition, the smaller perturbations tend to grow more rapidly, and to maintain their growth over a longer period, with the result that the DTE spans a range of two orders of magnitude after 6 h rather than the six orders of magnitude shown initially.

5. Summary and discussion

We have explored the growth of small-scale differences in simulations of the surprise East Coast snowstorm of 24–25 January 2000. Our approach is to calculate the difference evolution explicitly as the difference between a control simulation of MM5 and a simulation from perturbed initial conditions. In order to focus on the difference growth from small scales, the initial perturbation has the form of a monochromatic temperature perturbation of 85-km wavelength. We have considered both 30-km simulations in which moist convection is parameterized and triply nested simulations in which convection is explicitly, though marginally, resolved on the innermost 3.3-km grid.

At either resolution, differences grow rapidly at scales of 100–200 km over the first 6 h from the initial, 85-km wavelength perturbation and then, over the next 12 h, spread to larger scales while their growth slows. Moist convection (or its parameterization) is the key process that drives the rapid initial growth: the differences grow first in a small region of negative lifted index and potential instability over the Gulf Coast of Louisiana, and fake dry simulations without latent heat release exhibit greatly reduced growth. In the 3.3-km simulations, the error growth occurs initially on a timescale of about an hour and is associated with differences in the timing and location of individual convective cells. This timescale is consistent with the results of Islam et al. (1993), who considered the predictability of tropical radiative–convective equilibrium solutions with resolved moist convection. In the 30-km simulations, the initial growth is associated with thresholds in the convective parameterization (or in the explicit microphysical parameterizations, if no convective parameterization is used) and proceeds at a rate that increases as the initial error amplitude decreases. Although the difference evolution at coarse resolution qualitatively resembles that in the higher-resolution simulations, we emphasize that the convective parameterization is, at best, an ad hoc surrogate for resolved processes in its influence on error growth.

Upscale spreading of differences with time is evident both in physical and spectral representations of the differences. While this upscale spreading is associated in part with the spreading of differences over a larger physical area with time, it is also clear that after 24~30 h, differences are significantly influenced by balanced dynamics and have begun to appear in, for example, the subsynoptic-scale structure of the surface low. Our primary conclusion is that rapid growth at the convective scale, and subsequent upscale spreading of error, places severe constraints on the accuracy mesoscale forecasts. As suggested by Lorenz (1969), the fact that the timescale for the growth of convective-scale differences is about 1 h (or less; see below) means that even small differences in initial conditions can make significant differences in the 1–2-day forecast. Of course, the present study applies only to a single case of midlatitude cyclogenesis, and further work will be required to generalize these results and to quantify more precisely the limits of mesoscale predictability. Nevertheless, the present study suggests that, if analyses continue to improve, we will eventually reach the point that reducing the initial error by half (a very substantial improvement) extends our forecasts, at a given skill level, by only 1 h.

The question then becomes how far present forecast systems are from that point of diminishing returns. The results in this paper show that a 0.5-K temperature perturbation implies 36-h precipitation differences of 5 cm or more over a large portion of the domain. This strongly suggests that detailed deterministic precipitation forecasts, at least for this case, are impractical beyond 2 to 3 days, and that the predictability is limited, much as originally proposed by Lorenz (1969), by the increasingly rapid growth of differences at successively smaller scales.

In addition, the present experiments likely represent an upper bound on predictability of the real atmosphere. This is because convective scale motions are only marginally resolved in the 3.3-km solutions and thus remain excessively damped in the model solutions. With higher resolution, we expect initial growth of differences at the convective scale to be even faster than found here. Similar increase of growth rates has been found in the past for planetary- and synoptic-scale flow as model resolution increased and scales characteristic of error growth became better resolved (Charney et al. 1966; Smagorinsky 1969; Simmons et al. 1995).

At first glance, the increase of difference growth rates with resolution might seem inconsistent with the result of ZSR that increasing the model resolution provided a better simulation of this case. Further consideration, however, reveals that there is no contradiction: at lower resolution, simulations do not diverge as rapidly but that divergence is a poor approximation to the divergence of the model solution from the atmospheric state. At higher resolution, the forecast model is more accurate, and this is reflected both in improvement of the forecast from a given initial condition and in divergence of solutions that is more rapid and thus more closely approximates the growth of forecast error.

Adjoint techniques are a common way of diagnosing the growth of forecast differences [see Ehrendorfer et al. (1999), for example]. Although useful in many situations, such techniques depend on the assumption that the difference dynamics is linear. Because of this, they

will be unable to reproduce fully the evolution of forecast differences from the convective scale to larger scales that is present in our experiments. In the high-resolution simulations, the assumption of linear dynamics will fail quickly because of the rapid local growth of differences to significant amplitude; adjoint techniques will be unable to capture the slower growth at larger scales that follows the initial rapid growth. At 30-km resolution, the difficulty will be associated with the nonlinearity inherent in the physical parameterizations (Errico and Raeder 1999).

The rapid growth of forecast error from the convective scales also has implications for the parameterization of moist convection (and for subgrid-scale parameterizations in general). Consider a low-resolution model for which scales below 100 km are unresolved and therefore parameterized. We have shown that, for this surprise snowstorm case, simulations from initial conditions differing only at scales below 100 km diverge over time, particularly where moist convection is active, and that divergence is significant even at scales larger than 100 km. Typically, parameterizations are deterministic functions of the resolved scales. The low-resolution simulations hypothesized above would thus be unable to capture the divergence of solutions from initially unresolved differences—the initial conditions are identical, so the resulting simulations are also identical. In order to capture the forecast divergence, the low-resolution model needs to produce different realizations of the forecast from identical initial conditions on the resolved scale; that is, the parameterization should be stochastic. Techniques for incorporating a stochastic element into parameterizations are a topic of active research (Buizza et al. 1999; Lin and Neelin 2000).

We have emphasized the limitations on mesoscale forecasts produced by the rapid error growth associated with moist convection. At the same time, however, there remains substantial room for improving existing forecasts. These improvements can be realized by improving initial conditions on the synoptic and larger mesoscale, either through the use of nonconventional observations or more sophisticated assimilation techniques; by improving forecast models, particularly the physical parameterizations; and through probabilistic or ensemble forecasting schemes. Such schemes acknowledge that, while mesoscale forecasts of, say, precipitation may be inherently uncertain even in the short range, they retain a wealth of useful information about the intensity, organization, and likelihood of precipitation.

Acknowledgments. The authors are grateful to Chris Davis and two anonymous reviewers for their thorough and insightful reviews of the earlier manuscript. This study was supported by U.S. Weather Research Program.

REFERENCES

Anthes, R. A., Y. H. Kuo, D. P. Baumhefner, R. P. Errico, and T. W. Bettge, 1985: Predictability of mesoscale atmospheric motions. *Adv. Geophys.,* **28B,** 159–202.

Bluestein, H., 1993: *Observations and Theory of Weather Systems.* Vol. 2, *Synoptic-Dynamic Meteorology in Midlatitude,* Oxford University Press, 594 pp.

Boffetta, G., A. Celani, A. Crisanti, and A. Vulpiani, 1996: Predictability in two-dimensional decaying turbulence. *Phys. Fluids,* **9,** 724–734.

Buizza, R., M. Miller, and T. N. Palmer, 1999: Stochastic representation of model uncertainties in the ECMWF Ensemble Prediction System. *Quart. J. Roy. Meteor. Soc.,* **125,** 2887–2908.

Charney, J. G., R. G. Fleagle, H. Riehl, V. E. Lally, and D. Q. Wark, 1966: The feasibility of a global observation and analysis experiment. *Bull. Amer. Meteor. Soc.,* **47,** 200–220.

Dudhia, J., 1993: A nonhydrostatic version of the Penn State–NCAR Mesoscale Model: Validation tests and simulation of an Atlantic cyclone and cold front. *Mon. Wea. Rev.,* **121,** 1493–1513.

Ehrendorfer, M., and R. M. Errico, 1995: Mesoscale predictability and the spectrum of optimal perturbations. *J. Atmos. Sci.,* **52,** 3475–3500.

——, ——, and K. D. Raeder, 1999: Singular-vector perturbation growth in a primitive equation model with moist physics. *J. Atmos. Sci.,* **56,** 1627–1648.

Errico, R. M., and D. P. Baumhefner, 1987: Predictability experiments using a high-resolution limited area model. *Mon. Wea. Rev.,* **115,** 488–504.

——, and K. D. Raeder, 1999: An examination of the accuracy of the linearization of a mesoscale model with moist physics. *Quart. J. Roy. Meteor. Soc.,* **125,** 169–195.

Grell, G. A., 1993: Prognostic evaluation of assumptions used by cumulus parameterizations. *Mon. Wea. Rev.,* **121,** 764–787.

Islam, S., R. L. Bras, and K. A. Emanuel, 1993: Predictability of mesoscale rainfall in the Tropics. *J. Appl. Meteor.,* **32,** 297–310.

Kain, J. S., and J. M. Fritsch, 1990: A one-dimensional entraining/detraining plume model and its application in convective parameterization. *J. Atmos. Sci.,* **47,** 2784–2802.

Langland, R. H., M. A. Shapiro, and R. Gelaro, 2002: Initial condition sensitivity and error growth in forecasts of the 25 January 2000 East Coast snowstorm. *Mon. Wea. Rev.,* **130,** 957–974.

Leith, C. E., 1971: Atmospheric predictability and two-dimensional turbulence. *J. Atmos. Sci.,* **28,** 145–161.

——, and R. H. Kraichnan, 1972: Predictability of turbulent flows. *J. Atmos. Sci.,* **29,** 1041–1058.

Lilly, D. K., 1972: Numerical simulation studies of two-dimensional turbulence. II. Stability and predictability studies. *Geophys. Fluid Dyn.,* **4,** 1–28.

Lin, J. W.-B., and D. Neelin, 2000: Influence of a stochastic moist convective parameterization on tropical climate variability. *Geophys. Res. Lett.,* **27,** 3691–3694.

Lorenz, E. N., 1969: The predictability of a flow which possesses many scales of motion. *Tellus,* **21,** 289–307.

Mellor, G. L., and T. Yamada, 1982: Development of a turbulence closure model for geophysical fluid problems. *Rev. Geophys. Space Phys.,* **20,** 851–875.

Metais, O., and M. Lesieur, 1986: Statistical predictability of decaying turbulence. *J. Atmos. Sci.,* **43,** 857–870.

Reisner, J., R. J. Rasmussen, and R. T. Bruintjes, 1998: Explicit forecasting of supercooled liquid water in winter storms using the MM5 mesoscale model. *Quart. J. Roy. Meteor. Soc.,* **124,** 1071–1107.

Simmons, A. J., R. Mureau, and T. Petroliagis, 1995: Error growth and estimates of predictability from the ECMWF forecasting system. *Quart. J. Roy. Meteor. Soc.,* **121,** 1739–1771.

Smagorinsky, J., 1969: Problems and promises of deterministic extended-range forecasting. *Bull. Amer. Meteor. Soc.,* **50,** 286–311.

Snyder, C., T. M. Hamill, and S. Trier, 2003: Linear evolution of error

covariances in a quasigeostrophic model. *Mon. Wea. Rev.*, **131,** 189–205.
Toth, Z., and E. Kalnay, 1997: Ensemble forecasting at NCEP and the breeding method. *Mon. Wea. Rev.*, **125,** 3297–3319.
Vukicevic, T., and R. M. Errico, 1990: The influence of artificial and physical factors upon predictability estimates using a complex limited-area model. *Mon. Wea. Rev.*, **118,** 1460–1482.
Zhang, F., C. Snyder, and R. Rotunno, 2002: Mesoscale predictability of the ''surprise'' snowstorm of 24–25 January 2000. *Mon. Wea. Rev.*, **130,** 1617–1632.